Published in final edited form as:

Chem Biol Drug Des. 2015 November ; 86(5): 1036–1048. doi:10.1111/cbdd.12571.

Synthesis and Evaluation of Derivatives of the Proteasome Deubiquitinase Inhibitor b-AP15

Xin Wang[1], **Pádraig D'Arcy**[1], **Thomas R. Caulfield**[2], **Aneel Paulus**[3], **Kasyapa Chitta**[3], **Chitralekha Mohanty**[4], **Joachim Gullbo**[5], **Asher Chanan-Khan**[3], and **Stig Linder**[1,4,*]

[1]Department of Medical and Health Sciences, Linköping University, S-581 83, Linköping, Sweden

[2]Department of Molecular Neuroscience, Mayo Clinic, 4500 San Pablo Road South, Jacksonville, FL 32224, USA

[3]Department of Cancer Biology, Mayo Clinic, 4500 San Pablo Road South, Jacksonville, FL 32224, USA

[4]Cancer Center Karolinska, Department of Oncology and Pathology, Karolinska Institute, S-171 76 Stockholm, Sweden

[5]Department of Immunology, Genetics and Pathology, Section of Oncology, Uppsala University, S-75185, Uppsala, Sweden

Abstract

The ubiquitin–proteasome system (UPS) is increasingly recognized as a therapeutic target for the development of anticancer therapies. The success of the 20S proteasome core particle (20S CP) inhibitor bortezomib in the clinical management of multiple myeloma has raised the possibility of identifying other UPS components for therapeutic intervention. We previously identified the small molecule b-AP15 as an inhibitor of 19S proteasome deubiquitinase (DUB) activity. Building upon our previous data, we performed a structure–activity relationship (SAR) study on b-AP15 and identified VLX1570 as an analog with promising properties, including enhanced potency and improved solubility in aqueous solution. *In silico* modeling was consistent with interaction of VLX1570 with key cysteine residues located at the active sites of the proteasome DUBs USP14 and UCHL5. VLX1570 was found to inhibit proteasome deubiquitinase activity *in vitro* in a manner consistent with competitive inhibition. Furthermore, using active-site-directed probes, VLX1570 also inhibited proteasome DUB activity in exposed cells. Importantly, VLX1570 did not show inhibitory activity on a panel of recombinant non-proteasome DUBs, on recombinant kinases, or on caspase-3 activity, suggesting that VLX1570 is not an overtly reactive general enzyme inhibitor. Taken together, our data shows the chemical and biological properties of VLX1570 as an optimized proteasome DUB inhibitor.

Keywords

chalcone; deubiquitinase; *in silico* modeling; inhibitor; lead optimization; proteasome

*Corresponding author: Stig Linder, stig.linder@liu.se; stig.linder@ki.se.

Supporting Information: Additional Supporting Information may be found in the online version of this article:

The UPS is the main mechanism for the controlled degradation of damaged, un-needed, or short-lived proteins in eukaryotic cells. At its most basic level, the UPS consists of a tagging factor in the form of the small molecule ubiquitin and the proteasome, a large multisubunit destruction complex. Proteins destined for proteasome degradation are tagged with ubiquitin, an evolutionally conserved 76 amino acid polypeptide, via a series of enzymatic steps involving E1, E2, and E3 ubiquitin ligases (1). The 26S proteasome complex consists of a proteolytic 20S core particle (20S CP) typically associated with one or two 19S regulatory particles (19S RP). Proteins tagged with polyubiquitin chains are recognized and captured by ubiquitin receptors on the 19S RP, unwound by ATPase activity, and finally translocated into the barrel-like 20S CP, where they are degraded by the three distinct catalytic subunits of the proteasome (2). To facilitate this process, ubiquitin chains are generally removed by the action of DUB enzymes situated at the 19S RP prior to substrate translocation into the catalytic chamber of the 20S CP. Proteasome-associated DUBs are parts of a diverse family of approximately 80 functional DUBs that are divided into five classes based on conserved homology in the catalytic domains. Four of these families are cysteine proteases and one family consists of metalloproteases (3). Cancer cells in particular are extremely sensitive to disruptions in the UPS, presumably due to the high rates of protein turnover. Even small fluctuations in UPS activity can trigger severe proteotoxic stress, resulting in the accumulation of high molecular weight ubiquitinated proteins, apoptosis, and ultimately cell death (4,5). This dependency of cancer cells for a functioning UPS has been exploited by the recent development of UPS inhibitors. In particular, the approval of Bortezomib (Velcade®), a dipeptidyl boronic acid derivative that selectively inhibits the 20S CP, as a first-line treatment for multiple myeloma has highlighted the potential of targeting the UPS for cancer drug development (6,7).

We have previously identified the chalcone derivative b-AP15 as a small molecule that inhibits the activity of the proteasome deubiquitinases USP14 and UCHL5 (8). Exposure of cancer cells to b-AP15 results in the rapid accumulation of ubiquitinated proteins and an acute proteotoxic stress response without altering the proteolytic capacity of the 20S CP. The drug shows antineoplastic activity in a number of syngeneic and xenograft tumor models, including multiple myeloma at doses that were well tolerated (8,9). Importantly, b-AP15 induced cell death in multiple myeloma cells that had acquired resistance to bortezomib (9) raising the possibility of using proteasome DUB inhibitors in anticancer therapies to overcome acquired drug resistance. The structure of b-AP15 contains Michael acceptors that likely bind the cysteine residues in the active site of USP14 and UCHL5. This inhibitory effect of b-AP15 appears to be specific for proteasome DUBs as it does not inhibit total DUB enzymatic activity in cell extracts. There is growing recognition of the potential of proteasome DUB inhibitors as an anticancer therapy with several small molecule inhibitors of proteasome DUB activity described. A chalcone derivative (RA-9) with a similar structure to b-AP15 was recently described as an inhibitor of proteasome DUB activities (10). Furthermore, the curcumin analog AC17 was reported to inhibit proteasome DUB activity as well as display *in vivo* antineoplastic activity on lung carcinoma xenografts (11). Similar to b-AP15, both AC17 and RA-9 contain two α,β unsaturated carbonyls (i.e. Michael acceptors) conjugated in a larger system including aromatic rings, suggesting a common pharmacophore present in proteasome DUB inhibitors.

Although b-AP15 displays potent activity in both *in vitro* and *in vivo* assays, several chemical properties occlude its development for use in the clinical setting. b-AP15 shows limited solubility and stability in aqueous solution and requires high concentrations of Kolliphor EL in formulas for parenteral injections (8,9). In this report, we have evaluated the structure–activity characteristics of b-AP15 in an attempt to optimize both antitumor activity and chemical properties. From our analysis, the lead compound VXL1570 showed a similar target specificity and mechanism of action to b-AP15. Furthermore, the improved solubility of VLX1570 allows for the use of excipients, which are more suitable for clinical administration.

Methods and Materials

Materials

b-AP15, VLX1570, and other analogs were synthesized by OnTarget Chemistry AB (Uppsala, Sweden). 19S proteasome (E-366), ubiquitin vinyl sulfone (U-202), HA-ubiquitin vinyl sulfone (U-212) (Boston Biochem, Cambridge, MA, USA); 26S proteasome (VB2910), ubiquitin–rhodamine 110 (VB3008) (Viva Bioscience, Exeter, UK), IU1 (VB2240); anti-β actin (AC-15), 3-(4,5-dimethyl-2-thiazolyl)-2,5-diphenyl-2H-tetrazolium bromide, MTT (M2128) (Sigma-Aldrich, St Louis, MO, USA); anti-ubiquitin K48 (Apu2) (Millipore, Billerica, MA, USA); anti-USP14 (A300-920A) and anti-UCHL5 (A304-099A) (Bethyl Laboratories, Inc., Montgomery, TX, USA); anti-Mcl-1 (559027) (BD Pharmingen™, Franklin Lakes, NJ, USA); and anti-HA (12CA5) (Roche, Basel, Switzerland).

Methods

Cell culture—HCT116 colon carcinoma cells were maintained in McCoy's 5A modified medium/10% fetal calf serum; KMS11 cells were maintained in RPMI1640 medium supplemented with 10% fetal calf serum, and the proteasome reporter cell line MelJuSo-Ub^{G76V} -yellow fluorescent protein (YFP) (12) was cultured in Dulbecco's modified Eagle's medium/10% fetal calf serum. All cells were incubated at 37 °C in 5% CO_2. Cell viability was monitored using the FMCA assay (13) or using the MTT assay (14).

Western blot analysis—Cell extract proteins were resolved by 3–8% Tris-acetate or 4–12% SDS–PAGE gels (Invitrogen, Carlsbad, CA, USA) and transferred onto nitrocellulose membranes. Membranes were blocked in 5% non-fat milk and probed with primary antibodies overnight at 4 °C. Following washing in PBST, membranes were incubated with appropriate secondary antibodies. Proteins were visualized using ECL substrate.

Deubiquitinase enzymatic assays—Preparations of 26S proteasomes (1 nM) were pretreated with DMSO, VLX1570, or b-AP15 for 2 min in assay buffer (25 mM Tris, 5 mM $MgCl_2$, 10% glycerol, 0.05 mg/mL BSA, 2 mM ATP, and 1 mM DTT) before addition of Ubrhodamine. Fluorescence was monitored at 37 °C using Ex/Em = 490 nm/520 nm to read data every 10 second for 30 min using a TECAN infinite 200 instrument. For UbVS labeling of KMS 11 cells, we lysed cell pellets from control or treated cells with buffer (50 mM HEPES pH 7.4, 250 mM sucrose, 10 mM $MgCl_2$, 2 mM ATP, 1 mM DTT) on ice for 30 min and

removed debris by centrifugation. We labeled 25 μg of protein with 1 μM UbVS for 30 min at 37 °C. Samples were resolved by SDS–PAGE and subjected to immunoblotting. For UbVS labeling of proteasomes, we pretreated purified 19S proteasomes (50 nM) with DMSO, VLX1570, or b-AP15 (50 μM) for 10 min at room temperature, followed by labeling with 1 μM HA-UbVS for 30 min at 37 °C and by immunoblotting.

Caspase-3 enzyme activity—Caspase-3 activity was determined using SensoLyte® Homogeneous Rh110 Caspase-3/7 Assay kit (Eurogentec, Liege, Belgium). Briefly, different concentrations of VLX1570 were incubated with caspase-3 for 15 min at 37 °C before the addition of Rh110 caspase-3/7 substrate and then continuously measured on a fluorometric plate reader using Ex/Em = 490 nm/520 nm to record data every 1 min for 5 min. The final concentration of caspase-3 was 2 nM, and Ac-DEVD-CHO was used as a positive control.

Bacterial reverse mutation assay—The potential to induce reversion mutations in the histidine operon was assayed in the *Salmonella typhimurium* tester strains TA98, TA100, and in *Escherichia coli* strain WP2 uvrA as described. Mutation test was carried out using the preincubation method (30 min, 37 °C) with and without phenobarbital-5,6-benzoflavone-induced rat liver metabolic (S9) activation. These experiments were performed by Accelera, Nerviano, Italy.

Pharmacokinetics—Approximately 3 days before dosing and while under anesthesia (an aqueous mixture of ketamine, xylazine, and acepromazine, subcutaneously administered), male Sprague Dawley rats (6 weeks, supplied by Charles River Laboratories, Italia) were surgically prepared for serial blood samples collection. The animals were fitted with a flexible 3F-polyurethane cannula (Biomedica Greto; method of sterilization: ethylene oxide) implanted in the superior vena cava via the jugular vein. VLX1570 was administered in the vehicle as IV slow injection in a fixed time of 10 min via tail vein. The compound was dissolved in 50% PEG400/40% Tween-80/10% Kolliphor EL and then diluted with saline. The drug was injected at a final dose of 5 mg/kg during 10 min.

Hepatocyte metabolism—Pooled cryopreserved human hepatocytes (10-donor mix) were obtained from Celsis IVT (product numbers X008001 and M005052; Chicago, IL, USA). Samples were analyzed by LC/MS using a Waters ACQUITY UPLC system plus Waters Xevo G2 quadrupole time-of-flight MS and a Waters ACQUITY C18 column with guard filter. Ion chromatograms were extracted from the time-of-flight MS total ion chromatograms using calculated monoisotopic accurate masses (calculated using Waters MassLynx software for deprotonated molecule) with a 20-mDa window. The metabolites were mined from the data acquired from the last time-point, using software-aided data processing (MetaboLynx XS including structure-intelligent dealkylation tool and mass defect filter) with manual confirmation. Structures of the observed metabolites were tentatively identified using obtained accurate mass and fragment ion data. These studies were performed by Admescope Ltd., Oulu, Finland (investigator, Ari Tolonen; laboratory technicians, Birgitta Paldanius and Pirkko Hyvönen).

Computational docking—Initial docking for VLX1570 was performed using glide (v. 5.6) within the Schrödinger software suite (Schrödinger, LLC) (15). The starting

conformation of ligands was obtained by the method of Polak–Ribière conjugate gradient (PRCG) energy minimization with the Optimized Potentials for Liquid Simulations (OPLS) 2005 force field (16) for 5000 steps, or until the energy difference between subsequent structures was < 0.001 kJ/mol-Å (15). Our docking methodology has been described previously (17–19), and the scoring function utilized has been described (20). Briefly, to generate the grids for docking, molecular refracting molecules were removed from the USP14 or UCHL5 crystal structure (PDB Codes: 2AYO7 (21) and 3IHR (22), respectively) (15). Schrödinger's SiteFinder module focused the grid on the active site region surrounding residues Cys114 and Cys88 for USP14 and UCHL5, respectively. Using this grid, initial placement for VLX1570 was docked using the Glide algorithm within the Schrodinger suite as a virtual screening workflow (VSW). The docking proceeded from lower precision through SP docking and Glide extra precision (XP) (glide, v. 5.6; Schrödinger, LLC) (23,24). The top seeded poses were ranked for best scoring pose and unfavorable scoring poses were discarded. Each conformer was allowed multiple orientations in the site. Site hydroxyls, such as in serine and threonine residues, were allowed to move with rotational freedom. Docking scores were used for comparing top-ranked docking poses where the reactive carbonyl from VLX1570 is positioned near the catalytic cysteine from USP14 (Cys114) or UCHL5 (Cys88). We utilized the covalent docking method within Schrödinger suite to allow the carbonyl of the inhibitor to form linkage to the thiol at the –SH group via a likely Michael's addition reaction. Hydrophobic patches were utilized within the VSW as an enhancement. Top favorable scores from initial dockings of yielded ∼6 to 10 poses with the top pose selected, and from this, the best pose was used for experiments in covalent docking. XP descriptors were used to obtain atomic energy terms such as hydrogen bond interaction, electrostatic interaction, hydrophobic enclosure, and pi-pi stacking interaction that result during the docking run (23,24). Molecular modeling for importing and refining the X-ray structure and generation of VLX1570 small molecule structures, as well as, rendering of figure images were completed with Maestro, the built-in graphical user interface of the Schrödinger chemistry package (v. 5.6; Schrödinger, LLC).

Results

Structural activity/solubility investigations of b-AP15 analogs

b-AP15 is a chalcone derivative composed of a central six-membered piperidine-4-one ring and two flanking aryl groups linked to the central ring via two symmetrical and sterically accessible β-carbons (Figure 1A). In order to make b-AP15 more 'drug-like', we attempted to improve its solubility via the addition of more hydrophilic groups to the carbon skeleton. We initially added hydroxyls on the side aryls (VLX1554), but this resulted in a strong decrease in cytotoxicity in survival assays using HCT116 colon cancer cells (Figure 1B). This observation is presumably due to the decrease in the reactivity of the electrophilic β-carbons required for inhibitory activity (25). The addition of carboxyl groups at the 2-position of the piperidine ring resulted in compounds (VLX1502, VLX1508) that showed strongly impaired biological activity (Figure 1B). Changing the central ring structure from a piperidine to a bicyclic nortropinone (8-azabicyclo[3.2.1]octan-3-one) ring resulted in totally abolished cytotoxic activity (data not shown). In contrast, substitution of the piperidine (six-membered) to an azepane (seven-membered) ring resulted in a slight but significant increase

in biological activity (b-AP15/VLX1546; VLX1552/VLX1570; VLX1545/VLX1567) (Figure 1C). Variations in the addition of electron-drawing groups on the flanking aryls did not have a major impact on the activity of azepane ring-based compounds (Figure S1). Nitrogen groups placed in the para-position on the aryls were, however, associated with stronger activity than when placed in the meta- or ortho-positions (VLX1546/VLX1572; VLX 1535–1537) (Figure 1C,D, Figure S2). VLX1562, containing a free azepane ring nitrogen, showed somewhat lower potency than VLX1570, which contained an acrylamide at the same position (Figure 1C,D). Furthermore, changing the acrylamide of VLX1570 to an acetamide (VLX1571) also resulted in a loss of potency (Figure 1D).

The most potent azepane-based compound identified was VLX1570. Similar to b-AP15, VLX1570 showed limited solubility in aqueous solution. However, whereas b-AP15 required an excipient containing at least 5% Kolliphor EL for injection, VLX1570 remained stable in solutions containing 1% Kolliphor and 4% Tween-80 (both excipient mixtures also contained 5% PEG400), making it more suitable for intravenous injection. Similar to b-AP15, VLX1570 has an acrylamide attached to the nitrogen of the central ring. As acrylamide is potentially mutagenic (26), we examined the potential of VLX1570 to induce DNA mutations in an *in vitro* model. The potential to induce reversion mutations in the histidine operon in *Salmonella typhimurium* (strains TA98, TA100) and in *Escherichia coli* (strain WP2 uvrA) was tested both with and without phenobarbital-5,6-benzoflavone-induced rat liver metabolic (S9) activation. No significant increase in revertant colony numbers could be detected, either with or without metabolic activation (Tables S1 and S2), suggesting that VLX1570 and metabolized products are non-mutagenic. The significantly increased potency of VLX1570 compared to b-AP15 and the lower requirement for Kolliphor EL led us to select this compound for further studies.

Predicted interaction of UCHL5 with VLX1570 via *in silico* docking

The catalytic cysteine residue 88 of UCHL5 may be attacked by VLX1570 via a Michael's addition reaction. The compound fits deep into a wedge-like crevice inside UCHL5 that includes the following residues within 4 Å of the small molecule: Leu10, Trp58, Gln82, Asn85, Cys88 (covalent linkage), Ala162, Phe163, His164, Phe165, and Leu181. An electrostatic colored surface rendering for UCHL5 shows the fit of the top XP docked ligands prior to covalent bond formation (Figure 2A). The nitro-groups from VLX1570 participate in electrostatic interactions with the Asn and Gln residues and transient π-cloud interactions occur with the phenyl-substituted rings from VLX1570 (Figure 2B). His164 and carbonyl oxygen from VLX1570 have stabilizing interactions. The electrostatic surface for the covalently bound VLX1570 shows the tightly bound groove that the drug is inserted into while linked to Cys88 (Figure S3). The ligand interaction map gives a good indication of the key regions from UCHL5 that stabilize VLX1570 into the groove (Figure S4).

Predicted interaction of USP14 with VLX1570 via *in silico* docking

USP14 is predicted to bind the VLX1570 inhibitor via a Michael's addition reaction at the thiol of residue Cys114 with the electrophilic β-carbon of the small molecule (Figure 2C,D). The crevice for USP14 is deeper and includes the following residues within 4 Å of the small molecule VLX1570: Asn109, Asn112, Cys114, Tyr115, Gln197, Gln198, Asp199, Ser431,

Ser432, Ser433, Gly434, His435, Tyr436, and Lys454. The VLX1570 drug has a binding mode that would block access to the C-terminus of ubiquitin for binding with USP14, as visible in X-ray structure 2AYO7 and our model (Figure 2C; Figure S5). An electrostatic colored surface rendering for UCHL5 shows the fit of the top XP docked ligands prior to covalent bond formation. As with UCHL5, Asn and Gln interactions stabilize the nitro-substituted phenyl rings, while the His435 is not facing the β-carbon in this insertion pose for VLX1570. VLX1570 potentially could insert in a 180°-rotated orientation, such that VLX1570 faces the His435 similar to UCHL5, but the most optimal pose from docking gives this orientation (Figure 2C). The electrostatic surface for the covalently bound VLX1570 shows both a deep groove and interprotein interactions that the drug fits between while linked to Cys114 (Figure S5). The ligand interaction map provides information on the critical interactions with USP14 that stabilize VLX1570 into the pocket (Figure S6).

Thiol reactivity of the electrophilic β-carbons of VLX1570

The α, β-unsaturated carbonyls of this series of compounds are expected to interact with the thiolates of active site cysteines in DUBs by Michael's addition reaction (27). This reactivity suggests that thiol-containing compounds such as dithiothreitol (DTT) would impair the cytotoxic activity of the compounds by Michael's addition reaction, as shown for similar compounds (28,29). We indeed found that the addition of DTT to the culture medium reduced VLX1570 cytotoxicity (Figure 3). However, DTT had to be added in large molar excess to alleviate the cytotoxicity of the drug, showing that complex formation between VLX1570 and DTT is strongly shifted toward free molecules.

Analysis of metabolism and pharmacokinetics

The metabolic pattern of VLX1570 was investigated in human cryopreserved hepatocytes. The results suggested extensive metabolism or cellular uptake of the compound with only small amounts of parental drug detected after 2-h incubation. A total of 20 different metabolites were formed of which the Phase I metabolism included several hydrogenation (+2H) and hydroxylation reactions, and defluorination of the side aryls was also observed (Figure 4A, Table 1). Drug conjugates included those with S-glutathione (GSH), S-cysteinyl glycine, and S-cysteine. Many of these reactions occurred in conjunction with defluorination, suggesting aromatic substitution (on the aryls), and/or with oxygenation, suggesting a reaction involving the acrylamide moiety and its presumable epoxy metabolite. Surprisingly, quite few metabolites involving the α, β-unsaturated carbonyls were detected, suggesting that these elements might not be highly reactive or that the conjugates formed are reversible. VLX1570 showed a rapid half-life in rat plasma after injection (Figure 4B) with kinetics similar to that observed with the hit compound b-AP15 (25). A C_{max} of 30.8 ± 1.3 ng/mL was observed.

VLX1570 induces a similar cellular response as b-AP15

Blocking of proteasome function is known to induce the expression of a cellular chaperone response, induction of ER stress and oxidative stress (8,30–33). Microarray analysis showed that VLX1570 induces chaperone expression (HSPA6, HSPA1L, HSPA4L), the oxidative stress marker HMOX1 [known to be induced by bortezomib (34)], and the ER stress-associated marker DDIT3/CHOP in MCF7 cancer cells (Table S3). The gene expression

profile was similar to that induced by b-AP15 (Table S3, Figure S7). We also examined the response to VLX1571, an analog of VLX1570 where the acrylamide moiety on the azepane ring is substituted to an acetamide. The response to this compound was very similar to that of b-AP15 and VLX1570 (Table S3, Figure S7).

VLX1570 is a competitive inhibitor of proteasome DUB activity

The inhibition of 19S deubiquitinase activity was assayed *in vitro* using the substrate Ub-rhodamine. VLX1570 showed a similar IC_{50} (6.4 ± 2.2 μM) to b-AP15 (6.5 ±2.9 μM) in this assay. VLX1570 was somewhat more potent than b-AP15 when Ub-AMC was used as a substrate (VLX1570: 13.0 ± 2.7 μM; b-AP15: 16.8 ± 2.8 μM). The kinetic data were consistent with competitive enzyme inhibition (control reactions: V_{max} 77.0 ± 12.0 FLU/min/ng proteasome; reactions in the presence of 20 μM VLX1570: V_{max}: 72.5 ± 12.9 FLU/min/ng proteasome). The inhibition of the activity of individual proteasome deubiquitinases was determined using the activity probe ubiquitin vinyl sulfone (Ub-VS) (Figure 5A). VLX1570 and b-AP15 both inhibit USP14 and UCHL5 activity of 19S regulatory particles with the inhibition of USP14 being more pronounced (Figure 5A). The efficacy of *in vitro* inhibition of proteasome DUB activity by b-AP15 is approximately one magnitude lower compared to the inhibition of proteasome function in living cells, an apparent paradox that may be explained by enrichment of the drug in cells (25). VLX1570 was indeed found to inhibit USP14 in cells at a concentration of 1 μM (Figure 5B). In this assay, cells were exposed to VLX1570 and extracts were labeled with Ub-VS. Ub-VS is expected to compete with VLX1570 for substrate binding in extracts, resulting in difficulties to demonstrate inhibition, but the inhibition of labeling was consistent in triplicate samples. The inhibition of labeling of UCHL5 was less consistent in this type of assay as previously reported (25).

We examined the extent of polyubiquitin accumulation in HCT116 cells exposed to VLX1570 and compared it with other UPS inhibitors (Figure 5C). VLX1570 and b-AP15 induced similar levels of polyubiquitin; these levels were higher compared to those found in cells exposed to bortezomib. The average molecular weights of poly-ubiquitinated proteins were similar in cells exposed to b-AP15 and VLX1570 and higher compared to cells exposed to bortezomib (Figure 5C). This observation is consistent with a mechanism of DUB inhibition, as previously discussed (8). The USP14 inhibitor IU1 (35) induced weak accumulation of polyubiquitin after 18 h of exposure. WP1130 (Degrasyn) has been shown to inhibit USP14 and UCHL5 as well as other DUB enzymes (see below) (29). WP1130 induced polyubiquitin after 6 h, but not after 18 h (Figure 5C). This compound was strongly cytotoxic with few cells remaining at later time-points.

VLX1570 shows specificity to proteasome DUB activity

The Michael acceptor reactivity of b-AP15 and VLX1570 may be expected to lead to broad inhibitory activity toward cysteine proteases. However, we previously found that b-AP15 inhibited proteasome cysteine DUB activity without altering the activities of non-proteasome-associated cytosolic DUBs (8). To further confirm these findings, we performed a deubiquitinase profiling experiment using recombinant enzymes treated with VLX1570 (experiment was performed by Ubiquigent Ltd, Dundee, UK) (Figure 6A). Some inhibition of USP5 (~50%) was observed at a VLX1570 concentration of 20 μM; however, this

appeared to be the exception as the activity of most DUBs tested was not significantly inhibited.

We also examined whether VLX1570 inhibits an unrelated cysteine protease, caspase-3. We did not, however, detect the inhibition of caspase-3 at a concentration of 40 μ_M VLX1570 (Figure 6B). Finally, to further characterize the specificity and potential general reactivity of VLX1570, we determined the ability of the drug to inhibit a panel of kinases *in vitro* (Figure 6C). A kinase panel (211 separate enzymes) was tested for inhibition at a drug concentration of 10 μ_M, a standard concentration in kinase profiling experiments. Only one single kinase in the total panel was inhibited by > 50% (Cdk4), with the median level of inhibition being at 4% (Figure 6C).

The DUB inhibitor WP1130 contains an α, β-unsaturated carbonyl group and has been shown to inhibit USP14 and UCHL5, but also USP9x and USP5 (29). A decline in the levels of the anti-apoptotic protein MCL-1 in cells exposed to WP1130 was reported (29), presumably due to loss of deubiquitination of MCL-1 by USP9x (36). Decreased levels of MCL-1 were indeed observed following exposure of MelJuSo cells to WP1130, whereas this effect was not observed in HCT116 cells (Figure 7). Interestingly, however, MCL-1 levels increased when these two cell lines were exposed to b-AP15/VLX1570 (Figure 7). These findings are consistent with the finding that VLX1570 does not inhibit USP9x, and show that different DUB inhibitors containing α, β-unsaturated carbonyl groups, but are otherwise chemically unrelated, may elicit distinct biological effects.

Discussion

Proteasome inhibition has been established as a therapeutic treatment for multiple myeloma. We have previously shown that the proteasome DUB inhibitor b-AP15 displayed antitumor activity on multiple myeloma cells both *in vitro* and *in vivo* (9). Building on our previous hit compound, we performed a medicinal chemistry optimization of b-AP15 and found that compounds containing a central azepane ring were more potent than piperidine-based compounds. One of our primary motivations in performing this study was to obtain a lead compound more suited to administration in patients. In our previous *in vivo* studies with b-AP15, we employed a formulation containing 5% Kolliphor EL (previously known as Cremophor EL). As Kolliphor EL has been described to be associated with the development of hypersensitivity reactions (37), we attempted to find potent b-AP15 analogs that could be dissolved in excipients containing lower concentrations of Kolliphor EL and suitable for intravenous injections. The azepane derivative VLX1570 was found to be soluble at an adequate concentration in a formulation containing 5% PEG400/1% Kolliphor EL/4% Tween-80 (also known as Polysorbate-80) allowing the possibility for intravenous administration.

Similar to b-AP15, VLX1570 inhibits proteasome deubiquitinase activity and induces accumulation of high molecular weight polyubiquitinated proteins in cells. Analysis of enzyme inhibition showed that VLX1570 displays properties consistent with a mechanism of competitive inhibition of proteasome DUB activity. As VLX1570 contains α,β unsaturated dienones (i.e. Michael acceptors) that are expected to react with the cysteine in

the active sites of DUBs, a model of competitive inhibition is indeed expected. A chalcone derivative with a similar structure as b-AP15 (RA-9) was recently reported to inhibit proteasome deubiquitinase activity (10) (Figure S8). Interestingly, RA-9 induces endoplasmic reticulum stress, similar to what has been reported for b-AP15 (30), suggesting a common mechanism of action of both drugs. The 4-arylidene curcumin analog AC17, which also contains α,β unsaturated dienones (Figure S8), was recently found to inhibit the deubiquitinase activity of the 19S RP (11). All of these different DUB inhibitors are electrophiles and would *a priori* be expected to confer unspecific reactivity. However, b-AP15, RA-9, and AC17 have been shown not to inhibit total DUB activity in cell lysates (8,10,11). RA-9 was, however, found to inhibit UCHL1, UCHL3, and USP8 *in vitro* (38). Furthermore, the chalcone derivatives G5/F6 were reported as more broad specificity DUB inhibitors (39,40). We here examined of the ability of VLX1570 to inhibit cellular deubiquitinases using recombinant proteins (performed by Ubiquigent Ltd, Dundee). Remarkably, broad unspecific inhibition of the different DUBs in the panel was not observed. In addition, we also found that VLX1570 did not inhibit the non-DUB cysteine protease caspase-3. The basis for these differences in results using various chalcone analog and curcumin analog is unclear. Considering the expected cytotoxicity resulting from blocking of proteasome function, we believe it to be likely that the inhibition of proteasome DUBs (USP14/UCHL5) is of key importance to the biological effects of α,β-unsaturated ketone-containing compounds [for a further discussion, see (4)]. To further examine the potential general reactivity of VLX1570, we performed a screen for the inhibition of cellular kinases. VLX1570 is not a general kinase inhibitor by this analysis, showing a median level of inhibition of the panel of ~4% at 10 μM. The most strongly inhibited kinase was Cdk4, which was inhibited to ~80% by 10 μM VLX1570. In spite of the level of inhibition, Cdk4 inhibition is unlikely to be of importance for the activity of VLX1570 as embryonic fibroblasts proliferate normally in the absence of this kinase and mice devoid of Cdk4 are viable (41,42).

Docking for the bound VLX1570 models, we find support for a Michael's type addition reaction. In the case of USP14 and UCHL5, we see that both proteins have capacity to accommodate VLX1570 to dock; with USP14, the docked model has tyrosine and lysine available for stabilization at the charged nitrogens from $-NO_2$ groups, but dynamics would better access the long-term stabilization this confers. The fluoro-groups of VLX1570 are at the para-position and the nitro-groups are at the meta-position the phenyl rings. The tight binding prior to catalysis of the thiol linkage to the β-carbon of VLX1570 allows for stabilization needed to optimize binding likelihood. In the case of USP14, we see somewhat better protein–ligand interaction that increases likelihood of catalysis.

A general cysteine reactivity of b-AP15/VLX1570 may be predicted to lead to substance depletion due to binding to intracellular thiols. The cytotoxicity of other compounds containing α, β-unsaturated carbonyl groups are indeed inhibited by thiol-containing compounds such as dithiothreitol (DTT) (28,29). We found that VLX1570 shows a comparatively low reactivity to DTT, further supporting the notion that VLX1570 is not an overtly reactive compound. Electrophiles have been shown to target functional protein systems in a hierarchical manner (43,44). High-affinity targets are likely to consist of enzymes with catalytic cysteine that have a low pK_a due to the close proximity of

neighboring residues (such as histidines). The pK_a of the thiols of DTT is ~9.2 and GSH ~9.4 (45), explaining their low reactivities. We have also found that treatment with b-AP15 does not result in depletion of cellular glutathione (GSH) levels (C. Sun, unpublished data).

Conclusions

The results presented here show that VLX1570 has a mechanism of action that is indistinguishable from the hit compound b-AP15. b-AP15 was previously shown to be cytotoxic to numerous cancer types as well as to multiple myeloma cells resistant to the 20S proteasome inhibitor bortezomib, suggesting that proteasome DUB inhibitors may have clinical potential (9). VLX1570 has been granted IND status by the US Food and Drug Administration and is a candidate drug for the treatment of refractory multiple myeloma and will contribute to the therapeutic arsenal to treat cancer.

Supplementary Material

Refer to Web version on PubMed Central for supplementary material.

Acknowledgments

We are grateful to Marten Fryknäs and Rolf Larsson, Department of Medical Sciences, Uppsala University for discussions and for invaluable help with various analyses and for discussions. We are also grateful to Hans Rosén, Per Hag-mar (Vivolux AB, Mölndal), and Per Sjöberg (Euronia KB, Uppsala) for invaluable help and support. We are grateful to Maria Rydåker, Lena Lenhammar, and Christina Leek for excellent technical support. We acknowledge Admescope, Oulu, Finland, for the performance of LC/MS (pharmacokinetic studies) and metabolism studies and OnTarget Chemistry, Uppsala, Sweden, for synthesis of compounds. Grants were obtained from Cancerfonden, Vetenskåpsradet, Radiumhemmets forskningsfonder, Barncancerfonden, Strategiska Forskningsstiftelsen (SSF) and from Vivolux AB. SL and PD are shareholders in Vivolux AB. The experiments and analysis carried out in this study were supported in part by the University of Iowa/Mayo Clinic Lymphoma SPORE Developmental Research program (P50 CA097274, Aneel Paulus) and the Daniel Foundation of Alabama (Asher Chanan-Khan).

References

1. Hershko A, Ciechanover A. The ubiquitin system. Annu Rev Biochem. 1998; 67:425–479. [PubMed: 9759494]
2. Groll M, Ditzel L, Lowe J, Stock D, Bochtler M, Bartunik HD, Huber R. Structure of 20S proteasome from yeast at 2.4 A resolution. Nature. 1997; 386:463–471. [PubMed: 9087403]
3. Komander D, Clague MJ, Urbe S. Breaking the chains: structure and function of the deubiquitinases. Nat Rev Mol Cell Biol. 2009; 10:550–563. [PubMed: 19626045]
4. D'Arcy P, Wang X, Linder S. Deubiquitinase inhibition as a cancer therapeutic strategy. Pharmacol Ther. 2015; 147:32–54. [PubMed: 25444757]
5. D'Arcy P, Linder S. Molecular pathways: translational potential of deubiquitinases as drug targets. Clin Cancer Res. 2014; 20:3908–3914. [PubMed: 25085788]
6. Adams J. The development of proteasome inhibitors as anticancer drugs. Cancer Cell. 2004; 5:417–421. [PubMed: 15144949]
7. Richardson PG, Sonneveld P, Schuster MW, Irwin D, Stadtmauer EA, Facon T, Harousseau JL, et al. Bortezomib or high-dose dexamethasone for relapsed multiple myeloma. N Engl J Med. 2005; 352:2487–2498. [PubMed: 15958804]
8. DArcy P, Brnjic S, Olofsson MH, Fryknäs M, Lindsten K, De Cesare M, Perego P, Sadeghi B, Hassan M, Larsson R, Linder S. Inhibition of proteasome deubiquitinating activity as a new cancer therapy. Nat Med. 2011; 17:1636–1640. [PubMed: 22057347]

9. Tian Z, D'Arcy P, Wang X, Ray A, Tai YT, Hu Y, Carrasco RD, Richardson P, Linder S, Chauhan D, Anderson KC. A novel small molecule inhibitor of deubiquitylating enzyme USP14 and UCHL5 induces apoptosis in multiple myeloma and overcomes bortezomib resistance. Blood. 2013; 125:706–716. [PubMed: 24319254]
10. Coughlin K, Anchoori R, Iizuka Y, Meints J, MacNeill L, Vogel RI, Orlowski RZ, Lee MK, Roden RB, Bazzaro M. Small-molecule RA-9 inhibits proteasome-associated DUBs and ovarian cancer *in vitro* and *in vivo* via exacerbating unfolded protein responses. Clin Cancer Res. 2014; 20:3174–3186. [PubMed: 24727327]
11. Zhou B, Zuo Y, Li B, Wang H, Liu H, Wang X, et al. Deubiquitinase inhibition of 19S regulatory particles by 4-arylidene curcumin analog AC17 causes NF-kappaB inhibition and p53 reactivation in human lung cancer cells. Mol Cancer Ther. 2013; 12:1381–1392. [PubMed: 23696216]
12. Menendez-Benito V, Verhoef LG, Masucci MG, Dantuma NP. Endoplasmic reticulum stress compromises the ubiquitin-proteasome system. Hum Mol Genet. 2005; 14:2787–2799. [PubMed: 16103128]
13. Lindhagen E, Nygren P, Larsson R. The fluorometric microculture cytotoxicity assay. Nat Protoc. 2008; 3:1364–1369. [PubMed: 18714304]
14. Alley MC, Scudiero DA, Monks A, Hursey ML, Czerwinski MJ, Fine DL, Abbott BJ, Mayo JG, Shoemaker RH, Boyd MR. Feasibility of drug screening with panels of human tumor cell lines using a microculture tetrazolium assay. Cancer Res. 1988; 48:589–601. [PubMed: 3335022]
15. Mohamadi F, Richard NGJ, Guida WC, Liskamp R, Lipton M, Caufield C, Chang G, Hendrickson T, Still WC. Macromodel—an integrated software system for modeling organic and bioorganic molecules using molecular mechanics. J Comput Chem. 1990; 11:440–467.
16. Jorgensen WL, Tiradorives J. The opls potential functions for proteins – energy minimizations for crystals of cyclic-peptides and crambin. J Am Chem Soc. 1988; 110:1657–1666.
17. Caulfield T, Devkota B. Motion of transfer RNA from the A/T state into the A-site using docking and simulations. Proteins. 2012; 80:2489–2500. [PubMed: 22730134]
18. Loving K, Salam NK, Sherman W. Energetic analysis of fragment docking and application to structure-based pharmacophore hypothesis generation. J Comput Aided Mol Des. 2009; 23:541–554. [PubMed: 19421721]
19. Vivoli M, Caulfield TR, Martinez-Mayorga K, Johnson AT, Jiao GS, Lindberg I. Inhibition of prohormone convertases PC1/3 and PC2 by 2,5-dideoxystreptamine derivatives. Mol Pharmacol. 2012; 81:440–454. [PubMed: 22169851]
20. Friesner RA, Murphy RB, Repasky MP, Frye LL, Greenwood JR, Halgren TA, Sanschagrin PC, Mainz DT. Extra precision glide: docking and scoring incorporating a model of hydrophobic enclosure for protein-ligand complexes. J Med Chem. 2006; 49:6177–6196. [PubMed: 17034125]
21. Hu M, Li P, Song L, Jeffrey PD, Chenova TA, Wilkinson KD, Cohen RE, Shi Y. Structure and mechanisms of the proteasome-associated deubiquitinating enzyme USP14. EMBO J. 2005; 24:3747–3756. [PubMed: 16211010]
22. Burgie SE, Bingman CA, Soni AB, Phillips GN Jr. Structural characterization of human Uch37. Proteins. 2012; 80:649–654. [PubMed: 21953935]
23. Salam NK, Nuti R, Sherman W. Novel method for generating structure-based pharmacophores using energetic analysis. J Chem Inf Model. 2009; 49:2356–2368. [PubMed: 19761201]
24. Caulfield T, Medina-Franco JL. Molecular dynamics simulations of human DNA methyltransferase 3B with selective inhibitor nanaomycin A. J Struct Biol. 2011; 176:185–191. [PubMed: 21839172]
25. Wang X, Stafford W, Mazurkiewicz M, Fryknäs M, Brjnic S, Zhang X, Gullbo J, Larsson R, Arner ES, D'Arcy P, Linder S. The 19S deubiquitinase inhibitor b-AP15 is enriched in cells and elicits rapid commitment to cell death. Mol Pharmacol. 2014; 85:932–945. [PubMed: 24714215]
26. Dearfield KL, Douglas GR, Ehling UH, Moore MM, Sega GA, Brusick DJ. Acrylamide: a review of its genotoxicity and an assessment of heritable genetic risk. Mutat Res. 1995; 330:71–99. [PubMed: 7623872]
27. Mullally JE, Moos PJ, Edes K, Fitzpatrick FA. Cyclopentenone prostaglandins of the J series inhibit the ubiquitin isopeptidase activity of the proteasome pathway. J Biol Chem. 2001; 276:30366–30373. [PubMed: 11390388]

28. Liu JD, Tsai SH, Lin SY, Ho YS, Hung LF, Pan S, Ho FM, Lin CM, Liang YC. Thiol antioxidant and thiol-reducing agents attenuate 15-deoxy-delta 12,14-prostaglandin J2-induced heme oxygenase-1 expression. Life Sci. 2004; 74:2451–2463. [PubMed: 14998722]
29. Kapuria V, Peterson LF, Fang D, Bornmann WG, Talpaz M, Donato NJ. Deubiquitinase inhibition by small-molecule WP1130 triggers aggresome formation and tumor cell apoptosis. Cancer Res. 2010; 70:9265–9276. [PubMed: 21045142]
30. Brnjic S, Mazurkiewicz M, Fryknäs M, Sun C, Zhang X, Larsson R, D'Arcy P, Linder S. Induction of tumor cell apoptosis by a proteasome deubiquitinase inhibitor is associated with oxidative stress. Antioxid Redox Signal. 2014; 21:2271–2285. [PubMed: 24011031]
31. Fribley A, Wang CY. Proteasome inhibitor induces apoptosis through induction of endoplasmic reticulum stress. Cancer Biol Ther. 2006; 5:745–748. [PubMed: 16861900]
32. Fribley A, Zeng Q, Wang CY. Proteasome inhibitor PS-341 induces apoptosis through induction of endoplasmic reticulum stress-reactive oxygen species in head and neck squamous cell carcinoma cells. Mol Cell Biol. 2004; 24:9695–9704. [PubMed: 15509775]
33. Ling YH, Liebes L, Zou Y, Perez-Soler R. Reactive oxygen species generation and mitochondrial dysfunction in the apoptotic response to Bortezomib, a novel proteasome inhibitor, in human H460 non-small cell lung cancer cells. J Biol Chem. 2003; 278:33714–33723. [PubMed: 12821677]
34. Hamamura RS, Ohyashiki JH, Kurashina R, Kobayashi C, Zhang Y, Takaku T, Ohyashiki K. Induction of heme oxygenase-1 by cobalt protoporphyrin enhances the antitumour effect of bortezomib in adult T-cell leukaemia cells. Br J Cancer. 2007; 97:1099–1105. [PubMed: 17895889]
35. Lee BH, Lee MJ, Park S, Oh DC, Elsasser S, Chen PC, Gartner C, Dimova N, Hanna J, Gygi SP, Wilson SM, King RW, Finley D. Enhancement of proteasome activity by a small-molecule inhibitor of USP14. Nature. 2010; 467:179–184. [PubMed: 20829789]
36. Schwickart M, Huang X, Lill JR, Liu J, Ferrando R, French DM, Maecker H, O'Rourke K, Bazan F, Eastham-Anderson J, Yue P, Dornan D, Huang DC, Dixit VM. Deubiquitinase USP9X stabilizes MCL1 and promotes tumour cell survival. Nature. 2010; 463:103–107. [PubMed: 20023629]
37. Hennenfent KL, Govindan R. Novel formulations of taxanes: a review. Old wine in a new bottle? Ann Oncol. 2006; 17:735–749. [PubMed: 16364960]
38. Issaenko OA, Amerik AY. Chalcone-based small-molecule inhibitors attenuate malignant phenotype via targeting deubiquitinating enzymes. Cell Cycle. 2012; 11:1804–1817. [PubMed: 22510564]
39. Aleo E, Henderson CJ, Fontanini A, Solazzo B, Brancolini C. Identification of new compounds that trigger apoptosome-independent caspase activation and apoptosis. Cancer Res. 2006; 66:9235–9244. [PubMed: 16982768]
40. Nicholson B, Leach CA, Goldenberg SJ, Francis DM, Kodrasov MP, Tian X, Shanks J, Sterner DE, Bernal A, Mattern MR, Wilkinson KD, Butt TR. Characterization of ubiquitin and ubiquitin-like-protein isopeptidase activities. Protein Sci. 2008; 17:1035–1043. [PubMed: 18424514]
41. Tsutsui T, Hesabi B, Moons DS, Pandolfi PP, Hansel KS, Koff A, Kiyokawa H. Targeted disruption of CDK4 delays cell cycle entry with enhanced p27(Kip1) activity. Mol Cell Biol. 1999; 19:7011–7019. [PubMed: 10490638]
42. Rane SG, Dubus P, Mettus RV, Galbreath EJ, Boden G, Reddy EP, Barbacid M. Loss of Cdk4 expression causes insulin-deficient diabetes and Cdk4 activation results in beta-islet cell hyperplasia. Nat Genet. 1999; 22:44–52. [PubMed: 10319860]
43. Weerapana E, Wang C, Simon GM, Richter F, Khare S, Dillon MB, Bachovchin DA, Mowen K, Baker D, Cravatt BF. Quantitative reactivity profiling predicts functional cysteines in proteomes. Nature. 2010; 468:790–795. [PubMed: 21085121]
44. Codreanu SG, Ullery JC, Zhu J, Tallman KA, Beavers WN, Porter NA, Marnett LJ, Zhang B, Liebler DC. Alkylation damage by lipid electrophiles targets functional protein systems. Mol Cell Proteomics. 2014; 13:849–859. [PubMed: 24429493]
45. Tajc SG, Tolbert BS, Basavappa R, Miller BL. Direct determination of thiol pKa by isothermal titration microcalorimetry. J Am Chem Soc. 2004; 126:10508–10509. [PubMed: 15327286]

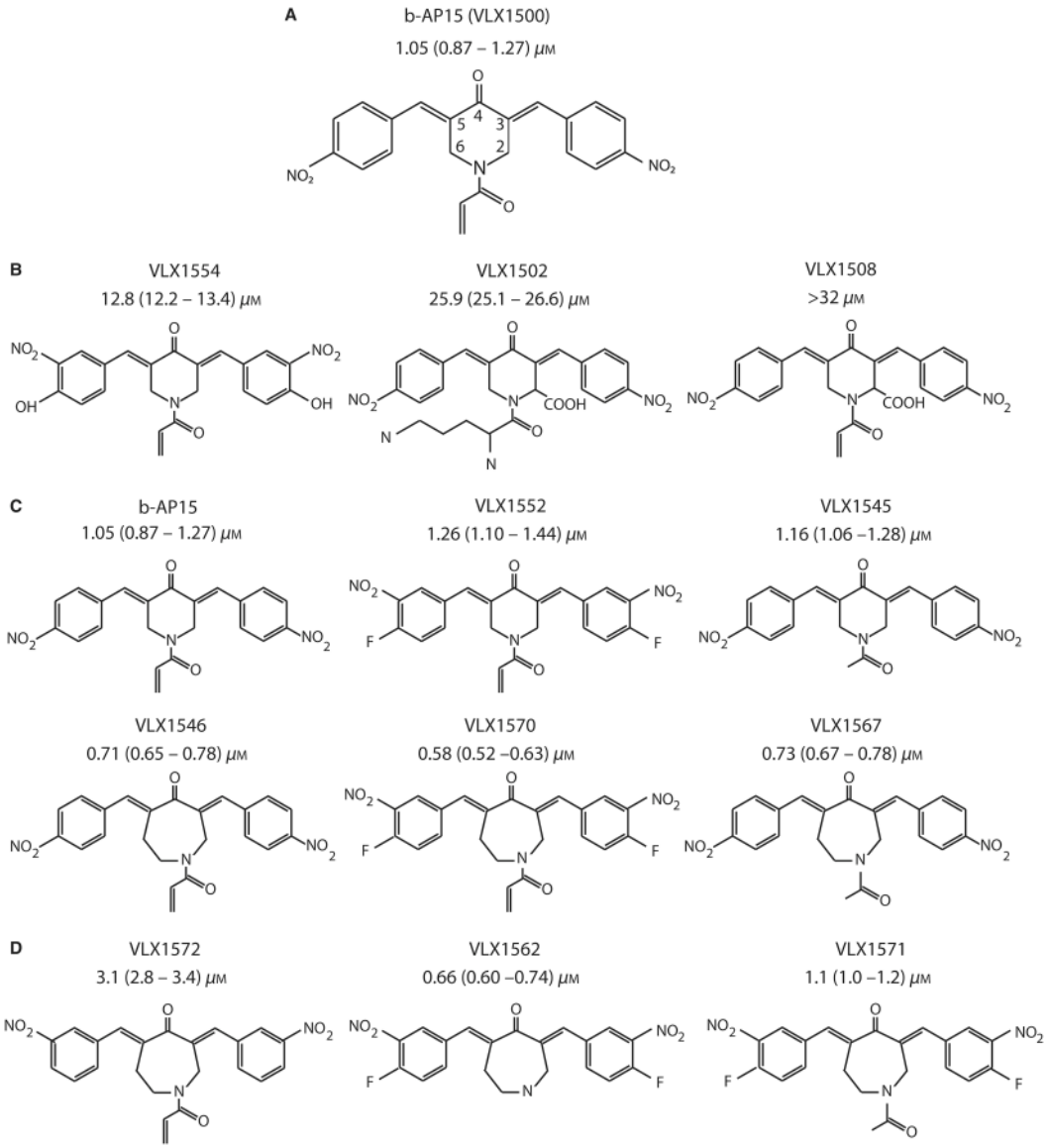

Figure 1.

Structure–activity relationships for b-AP15. (A) Structure of the DUB inhibitor lead b-AP15 (VLX1500); also shown is the IC_{50} value on HCT116 cells (CI: 95%). Cells were continuously exposed for 72 h and viability determined by FMCA. (B) Analogs containing hydroxyls on the side aryls or carboxyls in the piperidine ring. IC_{50} values from HCT116 cells (72-h exposure). (C) Pairwise comparisons of piperidine- and azepane-containing compounds. Shown are three pairs of compounds with azepane or piperidine central rings and the *in vitro* antiproliferative activities associated with these compounds. IC_{50} values from HCT116 cells (72-h exposure). (D) Effect of variations of the position on the nitro-group on the side aryls and varying the decoration of the nitrogen of the azepane ring. IC_{50} values from HCT116 cells (72-h exposure).

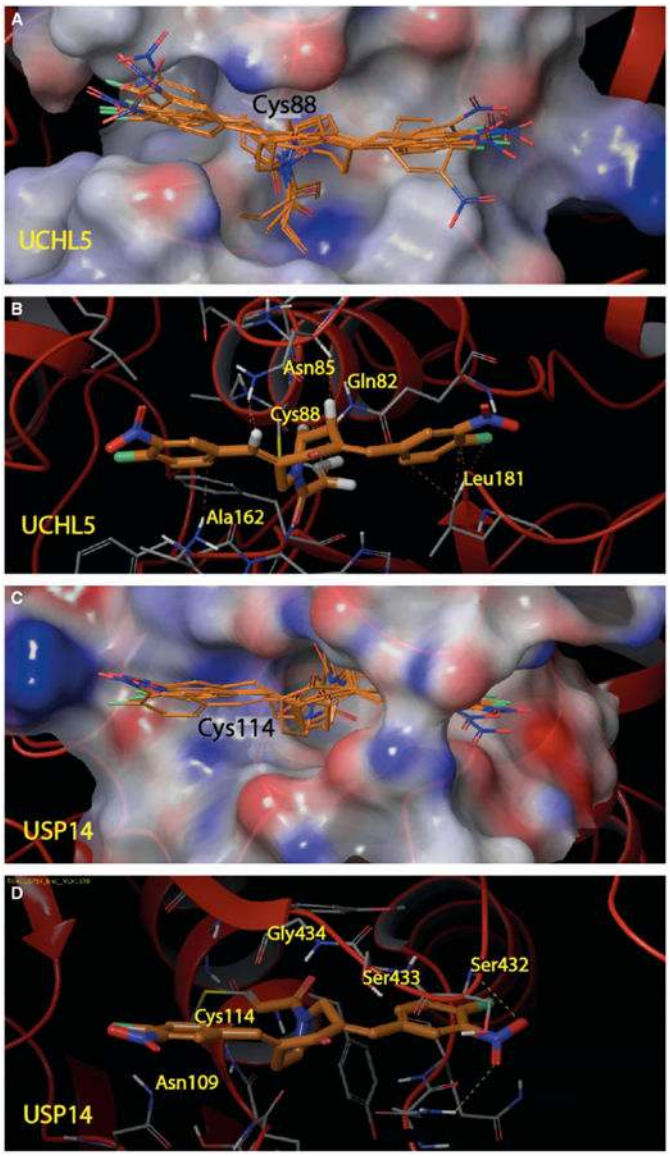

Figure 2.

In silico docking of VLX1570 with USP14 and UCHL5. (A) Precovalent docked poses of VLX1570 with UCHL5. Electrostatic colored surface for UCHL5 is shown to illustrate the crevice–groove, which VLX1570 occupies prior to catalytic linkage at the –SH thiol. (B) Covalent docked pose of VLX1570 with UCHL5. A molecular model for the predicted linkage between Cys88 and the VLX1570 β-carbon is shown. Important UCHL5 protein amino acid side chains with interaction with the VLX1570 molecule are labeled. Dashed lines indicate favorable interactions with drug and protein (VdW, H-bonds, or electrostatic). (C) Precovalent docked poses of VLX1570 with USP14. Electrostatic colored surface for USP14 is shown to illustrate the crevice–groove that VLX1570 occupies prior to catalytic linkage at the –SH thiol. (D) Covalent docked pose of VLX1570 with USP14. A molecular model for the predicted linkage between Cys114 and the VLX1570 β-carbon is shown.

Important USP14 protein amino acid side chains with interactions with VLX1570 are labeled.

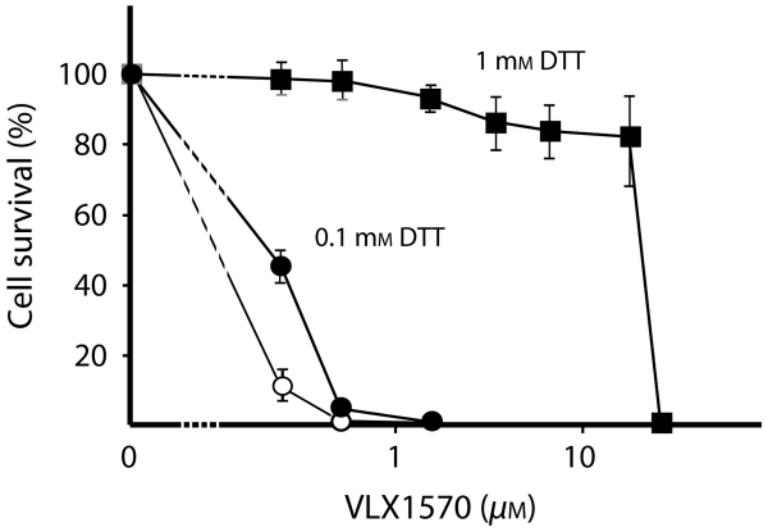

Figure 3.

DTT affects the cytotoxicity of VLX1570. MelJuSo-Ub^{G76V}-YFP cells were exposed to different concentrations of VLX1570 in the presence or absence of DTT (dithiothreitol) for 72 h. Cell viability was assessed using the MTT assay.

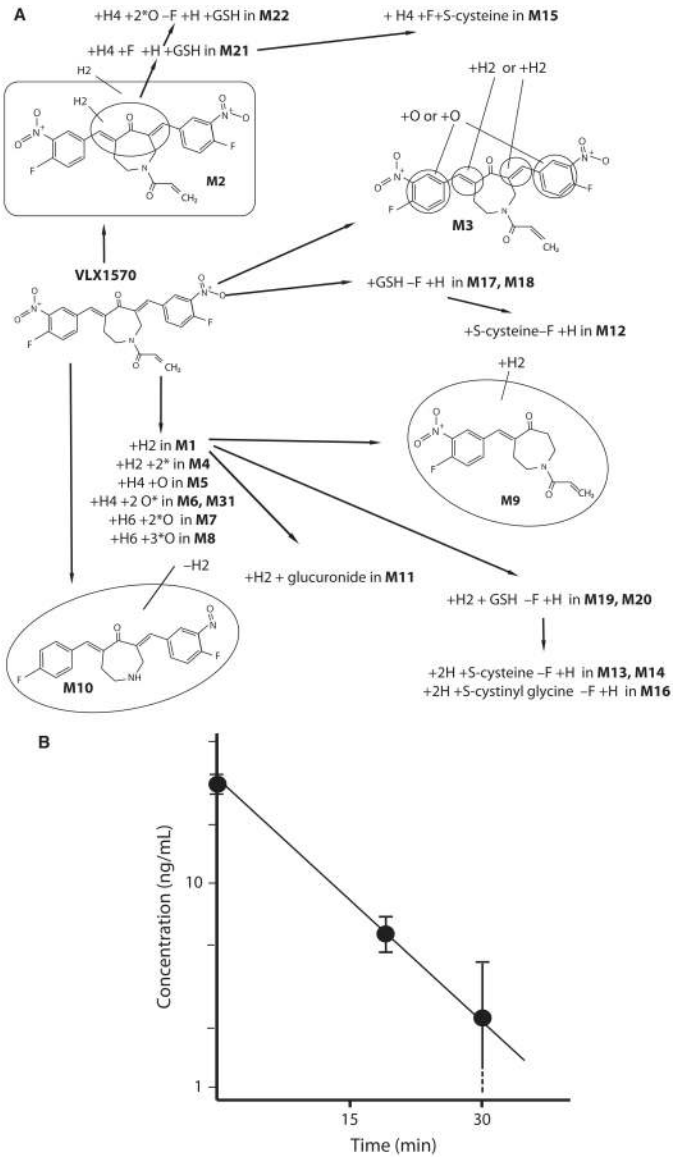

Figure 4.

(A) Metabolic pathways of VLX1570 in human cryopreserved hepatocytes. Hepatocytes were exposed to VLX1570 for 2 h, and metabolites were determined by LC/MS (see Materials and Methods). (B) Pharmacokinetics of VLX1570 in rats. VLX1570 was injected into Sprague Dawley rats (5 mg/kg) during 10 min. Plasma was collected after different times, and VLX1570 levels were determined by MS.

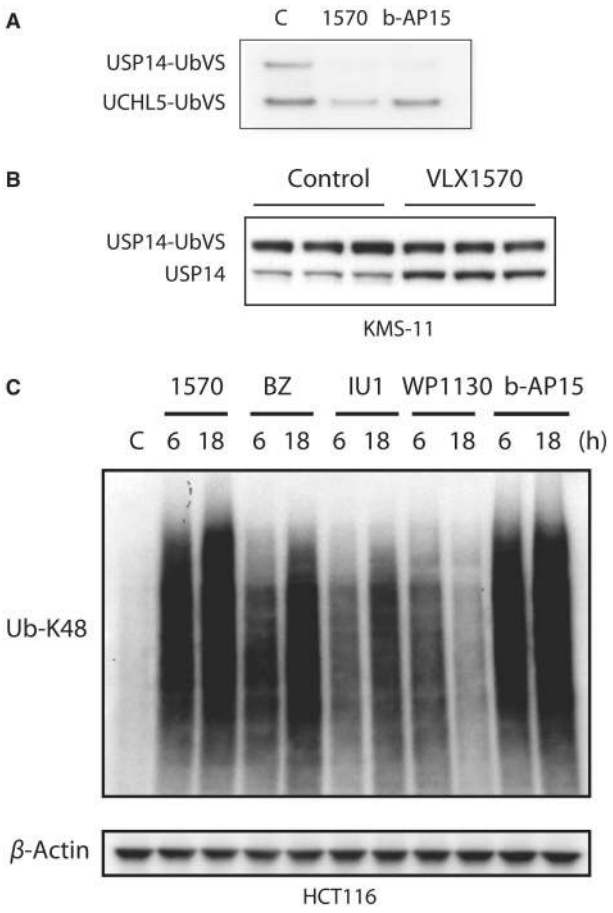

Figure 5.

(A) Inhibition of active-site-directed labeling of proteasome deubiquitinases. Purified 19S proteasomes (5 nM) were pre-treated with DMSO, VLX1570, and b-AP15 (50 μM) for 10 min at room temperature, followed by labeling with HA-UbVS and immunoblotting. (B) Inhibition of Ub-VS labeling of USP14 by VLX1570 in exposed cells. KMS-11 myeloma cells were treated with 1 μM VLX1570 for 6 h and 25 μg protein from whole-cell lysates were subsequently labeled with Ub-VS (1 μM), followed by SDS gel electrophoresis and immunoblotting with an USP14 antibody. Shown are triplicate samples of cells exposed to solvent or VLX1570. The lower band represents inactive USP14 enzyme. (C) Induction of polyubiquitin conjugates in KMS-11 myeloma cells. Cells were exposed to DMSO, 1 μM VLX1570, 100 nM bortezomib, 100 μM IU1, 5 μM WP1130, or 1 μM b-AP15 for 6 and 18 h, extracts prepared and subjected to immunoblotting with the indicated antibodies.

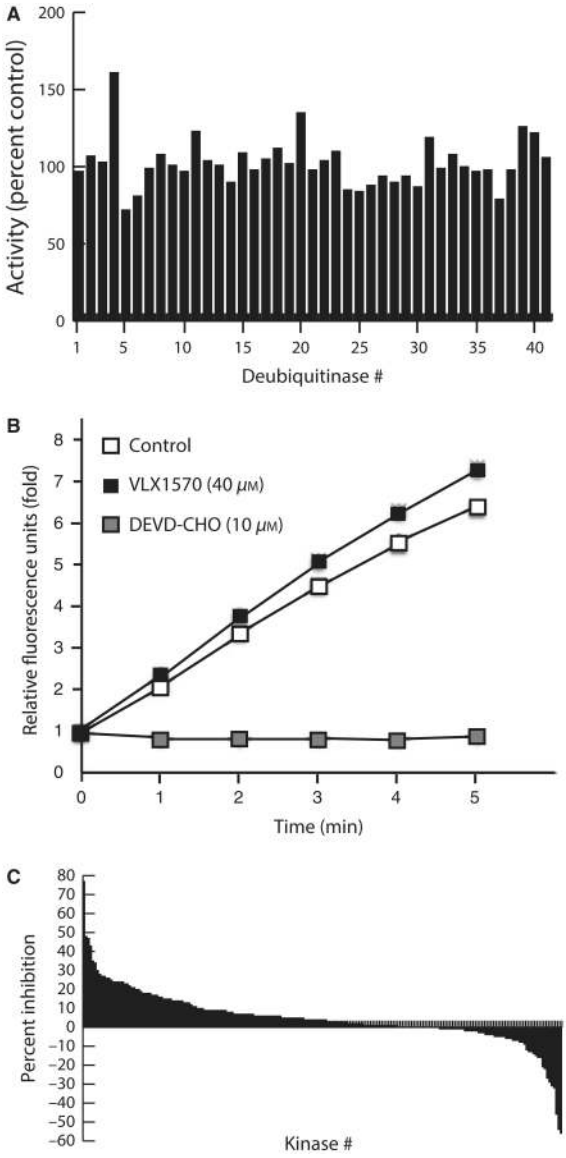

Figure 6.

(A) Determination of deubiquitinase inhibition by VLX1570. The following recombinant deubiquitinases were tested with regard to inhibition of activity by 20 μM. The tested DUBs were: 1. USP1; 2. USP2; 3. USP4; 4. USP5; 5. USP5 (+Ub@Kd); 6. USP5 (+Ub@Bmax); 7. USP6; 8. USP7; 9. USP8; 10. USP9x; 11. USP11; 12. USP14 (PS-VS@Kd); 13. USP15; 14. USP16; 15. USP19; 16. USP20; 17. USP21; 18. USP25; 19. USP28; 20. USP30; 21. USP35; 22. USP36; 23. USP45; 24. CYLD; 25. UCHL1; 26. UCHL3; 27. UCHL5; 28. BAP1; 29. OTU1; 30. OTUB2; 31. OTUD3; 32. OTUD5; 33. OTUD6A; 34. OTUD6B; 35. Cezanne; 36. AMSH-LP; 37. AMSH-LP (+Zn); 38. Ataxin3; 39. Ataxin3L; 40. JOSD1; 41. JOSD2. Note that USP14 was not inhibited under conditions where the enzyme was reconstituted with Ub-vinyl sulfone-treated proteasomes. Experiment was performed by Ubiquigent (http://www.ubiquigent.com). (B) *In vitro* inhibition of caspase-3 activity. VLX1570 (40 μM) or DEVD-CHO (10 μM) was incubated with caspase-3 prior to the addition

of Rh110 caspase-3/7 substrate, and the fluorometric signal was measured every minute for 5 min. (C) Determination of kinase inhibition by VLX1570. The enzymatic activities of 211 different kinases were determined in the presence of absence of 10 μ_M VLX1570. The 5 most strongly inhibited kinases were CDK4 (cyclin-dependent kinase 4) (77% inhibition), CaMK4 (48%), FLT-4 (VEGFR3) (47%), NEK4 (43%), and NDR1 (35%). Experiment was performed by CEREP (http://www.cerep.fr).

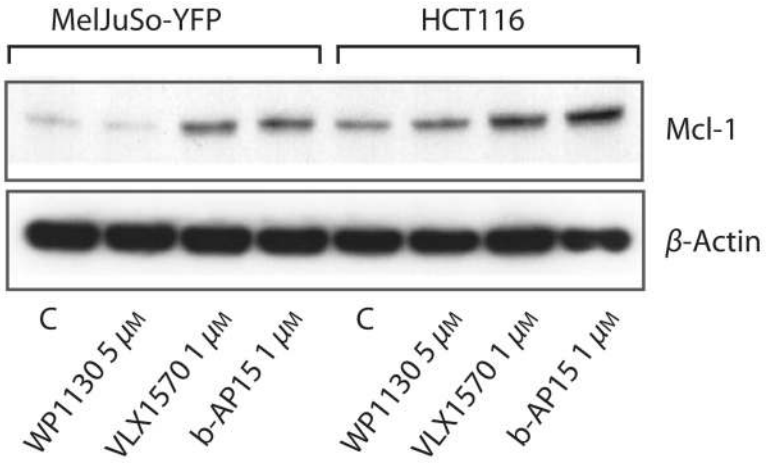

Figure 7.

MelJuSo-YFP and HCT116 cells were exposed to 5 μM WP1130, 1 μM VLX1570, or 1 μM b-AP15 for 4 h, cell extracts prepared and subjected to immunoblotting with Mcl-1 and β-actin antibodies.

Table 1

Relative LC/MS peak areas for VLX1570 and its metabolites in human hepatocytes, assuming identical LC/MS response between all compounds

	Area %
Parent	10.2
M1	3.2
M2	1.5
M3	11.1
M4	1.6
M5	2.7
M6	2.2
M7	4.2
M8	1.5
M9	1.5
M10	0.5
M11	1.4
M12	3.7
M13	7.4
M14	9.7
M15	4.0
M16	1.4
M17	3.7
M18	10.3
M19	10.1
M20	6.6
M21	0.9
M22	0.7